ACS SENSORS

pubs.acs.org/acssensors Article

# Wireless Tags with Hybrid Nanomaterials for Volatile Amine Detection

Rafaela S. Andre,* Quynh P. Ngo, Lucas Fugikawa-Santos, Daniel S. Correa,* and Timothy M. Swager*

Cite This: *ACS Sens.* 2021, 6, 2457–2464 Read Online

ACCESS | Metrics & More | Article Recommendations | Supporting Information

**ABSTRACT:** Quality control in the production and processing of raw meat is currently one of the biggest concerns for food industry and would benefit from portable and wireless sensors capable of detecting the onset of spoilage. Raw meat is a natural source of biogenic and volatile amines as byproducts of decarboxylation reactions, and the levels of these compounds can be utilized as quality control parameters. We report herein a hybrid chemiresistor sensor based on inorganic nanofibers of $SiO_2$:ZnO (an *n*-type material) and single-walled carbon nanotubes functionalized with 3,5-dinitrophenyls (a *p*-type material) with dosimetric sensitivity ~40 times higher for amines than for other volatile organic compounds, which also provides excellent selectivity. The hybrid nanomaterial-based chemiresistor sensory material was used to convert radio-frequency identification tags into chemically actuated resonant devices, which constitute wireless sensors that can be potentially employed in packaging to report on the quality of meat. Specifically, the as-developed wireless tags report on cumulative amine exposure inside the meat package, showing a decrease in radio-frequency signals to the point wherein the sensor ceased to be smartphone-readable. These hybrid material-modified wireless tags offer a path to scalable, affordable, portable, and wireless chemical sensor technology for food quality monitoring without the need to open the packaging.

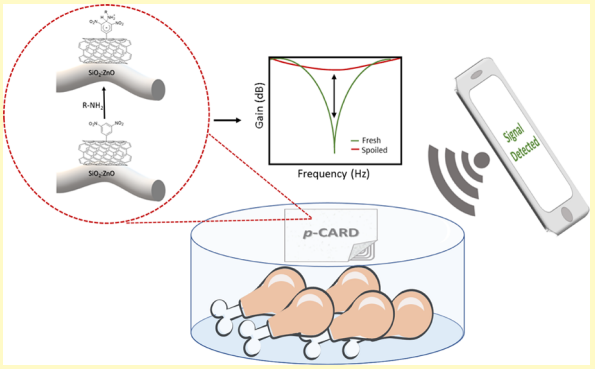


**KEYWORDS:** *inorganic nanofibers, carbon nanotubes, amine sensing, wireless sensing, radio-frequency identification*

Downloaded via MASSACHUSETTS INST OF TECHNOLOGY on June 27, 2021 at 13:42:19 (UTC).
See https://pubs.acs.org/sharingguidelines for options on how to legitimately share published articles.

## INTRODUCTION

Sensors for detecting volatile compounds are in high demand nowadays once some of them can present toxicity.[1−3] This is the case of volatile amines, which are widely used in pharmaceutical and chemical industries and can cause severe injuries such as eye and skin irritation and tearing.[4,5] In addition to the toxicity concerns, the monitoring of volatile amine emissions is important for food and beverage quality determination.[6,7] In particular, biogenic amine formation in food products is a robust indicator of the quality and state of preservation.[8] Biogenic amines are generally present in low concentrations and are natural metabolic compounds in a number of food products. These compounds are formed by enzymatic activity in raw meats and/or are produced by microbial decarboxylation of amino acids during storage. The most significant biogenic amines found in foods and beverages are histamine, putrescine, cadaverine, spermine, and spermidine.[5] When consumed in high concentration, biogenic amines cause diarrhea, vomiting, respiratory difficulties, and even neurotransmission disorders as a result of their ability to behave as false neurotransmitters.[9,10] Raw meat-based products would benefit from smart packages capable of monitoring the quality and preventing spoiled food consumption through preemptive volatile amine detection.[11,12] Wireless chemical sensing platforms are ideal for smart food and beverage packaging to ensure food safety.[13,14]

Wireless communication integrated with chemical sensors will have increasing significance in the future, allowing the sensing platform to be physically separated from data acquisition, readout, and computational resources.[15] Wireless chemical sensors have great versatility and can be used to safely monitor isolated, remote, and hazardous environments.[15,16] The integration and specifications of a chemical sensor with a wireless technology depend on the intended application, connectivity requirements, signal transduction features, and acceptable limitations.[17,18] The most common wireless technologies used in chemical sensing are Bluetooth, representing 34%, followed by radio-frequency identification (RFID), with 29% share, and ZigBee, representing 15% of total wireless technologies presently used.[18] RFID deserves special attention as a result of its power requirements, which can result

Received: April 19, 2021
Accepted: June 1, 2021
Published: June 10, 2021

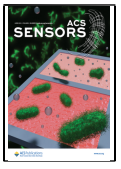


© 2021 American Chemical Society

https://doi.org/10.1021/acssensors.1c00812
*ACS Sens.* 2021, 6, 2457–2464

**Scheme 1. Schematic Representation of $Sio_2$:Zno Ceramic Nanofibers Combined with Single-Walled Carbon Nanotubes Functionalized with 3,5-Dinitrophenyl Groups (NF/DNP-CNT) Deposited in Parallel to the Existing Circuit (*P*) of a Commercially Available RFID Tag (*p*-CARD) and Its Radio-Frequency Signal Response over Exposure to Ammonia Derivatives**

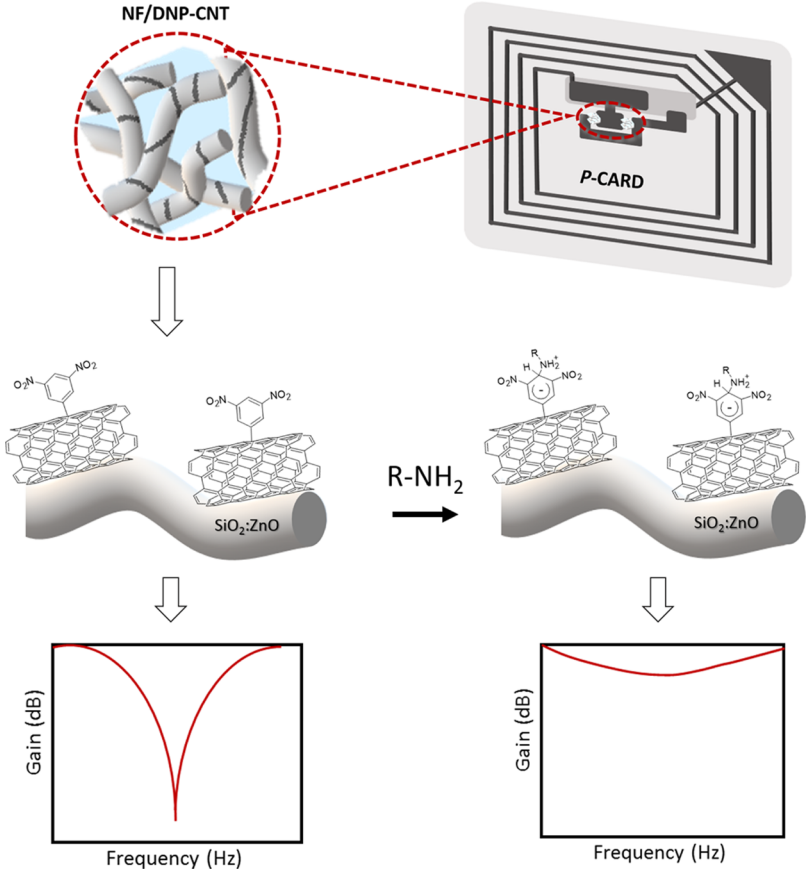


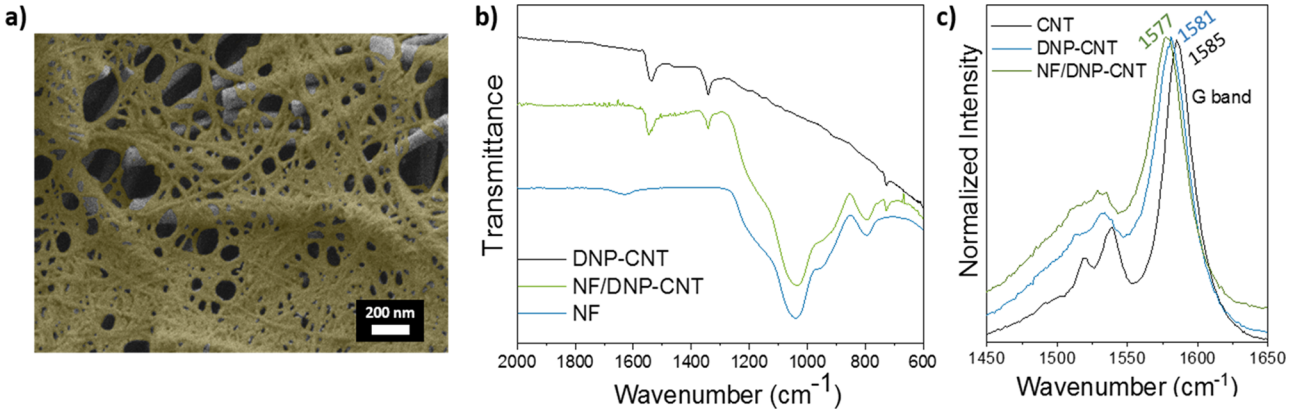


**Figure 1.** (a) SEM image of $SiO_2$:ZnO nanofibers (larger light gray fibers) combined with DNP-CNT (light brown structures) as a hybrid chemiresistor composition (NF/DNP-CNT). (b) FTIR spectra of DNP-CNT (black), NF/DNP-CNT (green), and pristine SiO2:ZnO NF (blue). (c) Raman spectra of pristine SWCNT (black), DNP-CNT (blue), and NF/DNP-CNT (green).

in low-cost passively powered devices, and the capability of incorporating and transmitting measured data (e.g., environmental characteristics) without physical contact between the tag and the RF reader. RFID wireless communication is based on coupling of electromagnetic waves and fields and can operate at a low frequency (9−135 KHz), high frequency (13.55−15.567 MHz), or ultrahigh frequency (2.45−5.8 GHz).[19] RFID technology is also widely implemented in logistics and in access control. Commercially available RFID tags can be converted into chemically actuated resonant devices (CARDs), and modification of the resonant circuit of passive tags with chemoresistive materials creates smartphone-readable sensors.[20−22]

We converted wireless RFID tags into CARD sensors by adding a composite of $SiO_2$:ZnO ceramic nanofibers (NF) and single-walled carbon nanotubes functionalized with 3,5-dinitrophenyl groups (DNP-CNT), as shown in Scheme 1. Functionalized CNT that have chemiresistor properties had


https://doi.org/10.1021/acssensors.1c00812
ACS Sens. 2021, 6, 2457−2464

previously been shown to be effective in creating CARD gas sensors.[21,23] It has also been previously shown that a combination of carbon nanotubes and inorganic metal oxides can provide improved performance as chemiresistive gas sensors.[24] Herein, we combine metal oxide NF, DNP-CNT, and passive RFID tags to create dosimetric sensors and detail their sensitivity to amines according to the degree of substitution at the amine and alkyl chain length. We have found that *n*-butylamine gives a particularly strong signal and this analyte was employed in the NF/DNP-CNT chemiresistor characterization and development of the extension to the smartphone-readable CARD sensors for the detection of biogenic amines in meat packaging. The dosimetric nature of the sensors provides high sensitivity and is appropriate to determine the quality of meat.

## RESULTS AND DISCUSSION

Our amine chemiresistive dosimeters are based on hybrid composition of $SiO_2$:ZnO semiconductor ceramic nanofibers and DNP-CNT, as presented in Scheme 1. The DNP group is known to react with primary amines to produce zwitterionic Meisenheimer complexes.[25,26] The DNP-CNT functionalization was characterized by XPS (described in the Supporting Information (SI) material, Section 1.2, Figure S4), indicating successful functionalization of SWCNT with a 3/100 ratio (3 DNP per 100 CNT). Pristine $SiO_2$:ZnO nanofibers were characterized by SEM and EDS, confirming the 1D morphology and expected element composition, as presented in Figure S5, and XRD in Figure S5c. The amorphous character of $SiO_2$ is evidenced by a broad band between 15 and 35°, while a ZnO feature is observed at 36.1°, which is attributed to the preferred diffraction plane (101) of the hexagonal zincite crystalline structure (JCPDS n° 36-1451).[27−29] The SEM image of NF/DNP-CNT, shown in Figure 1a, confirms that the $SiO_2$:ZnO nanofibers (larger gray structures) and the modified carbon nanotubes (light brown structures) create an interconnected porous NF/CNT network.[30] The FTIR spectra of DNP-CNT, pristine $SiO_2$:ZnO NF, and NF/DNP-CNT are presented in Figure 1b. DNP-CNT spectra (black line) show two peaks at 1538 and 1340 $cm^{-1}$ related to the asymmetric and symmetric stretch, respectively, of N−O from the dinitro group.[31,32] $SiO_2$:ZnO NF spectra present two bands around 1040 and 800 $cm^{-1}$ associated to the symmetric and asymmetric Si-O-Si vibrational stretch and a shoulder at 940 $cm^{-1}$ related to surface silanol (Si−OH) groups,[33−35] corroborating the presence of the silica matrix. NF/DNP-CNT spectra present all vibrational modes related to DNP-CNT and $SiO_2$:ZnO NF with a N−O peak shifted from 1538 to 1546 $cm^{-1}$, suggestive of van der Waals interactions between the $SiO_2$:ZnO NF and DNP-CNT in the hybrid material.[36,37] Raman spectroscopy was employed to evaluate the SWCNT's characteristic G-band, corresponding to an $sp^2$ C−C stretching mode, for the unfunctionalized CNT, DNP-CNT, and the NF/DNP-CNT composite. The Raman spectrum (Figure 1c) shows a 4 $cm^{-1}$ G-band shift to lower frequency after SWCNT functionalization with DNP and another 4 $cm^{-1}$ shift for the hybrid NF/DNP-CNT material, both for lower wavenumbers. A G-band shift to lower wavenumbers is observed when nanotubes interact with n-dopants.[38] This small shift suggests that both DNP groups and $SiO_2$:ZnO nanofibers increase electron density to the CNT. The electrical properties of $SiO_2$:ZnO NF, DNP-CNT, and NF/DNP-CNT were evaluated through electrical impedance measurements (Figure S6), revealing a synergistic effect between the $SiO_2$:ZnO NF and DNP-CNT. The Nyquist plot of NF/DNP-CNT (Figure S6c) shows a capacitive pattern, corroborating with the one observed for DNP-CNT (Figure S6b). However, the electrical resistance represented by a parallel R/C increases 5 times relative to DNP-CNT upon forming a composite with $SiO_2$:ZnO NF (Figure S6d), as expected when *p*-type CNT are combined with *n*-type materials.[39]

To evaluate the sensitivity to amines, pristine SWCNT, pristine $SiO_2$:ZnO NF, DNP-CNT, and NF/DNP-CNT were tested with exposure to *n*-butylamine at 50 ppm for 1 min (light gray area in Figure 2a). The response based on DNP-

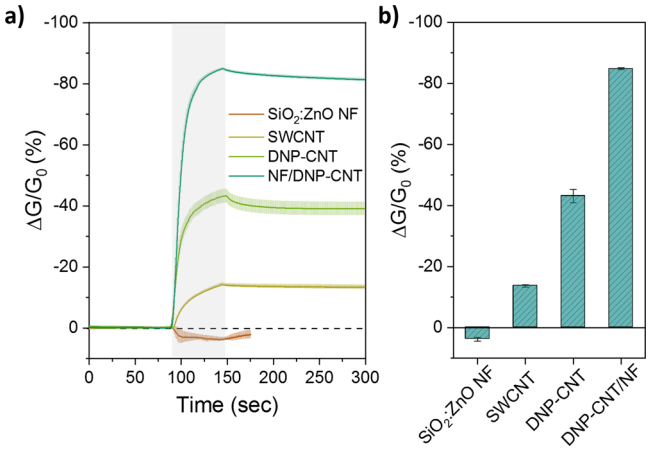


**Figure 2.** (a) Dynamic curve of amine-sensing response for $SiO_2$:ZnO NF, SWCNT, DNP-CNT, and NF/DNP-CNT for a 1 min of exposure to 50 ppm *n*-butylamine. (b) Average device response ($n \geq 4$) for pristine and hybrid chemiresistors.

CNT conductance is in accord with that expected for a *p*-type semiconductor (Figure 2b) and is more than 3 times higher than that observed for pristine, indicating the higher amine affinity imparted by the DNP groups.[25,26] Pristine $SiO_2$:ZnO nanofibers have an inverse response pattern characteristic of *n*-type materials when exposed to the reducing amine vapor.[40−42] The hybrid chemiresistor composition (NF/DNP-CNT) shows an improved response, 8 times higher than that of the pristine SWCNT and double that of the DNP-CNT. Similar to DNP-CNT, NF/DNP-CNT sensitivity is governed by DNP affinity to amines, leading to the formation of Meisenheimer complexes, as presented in Scheme 1. The Meisenheimer complex formation could be corroborated by FTIR measurements, presented as Figure S7, which shows that the N−O stretch at 1538 $cm^{-1}$ shifts to 1490 $cm^{-1}$ after exposure to amine vapor.[43] The overall improved sensor response is a consequence of the synergistic effect between NF/DNP-CNT constituents. The interaction of amines with the DNP group induces changes in the CNT charge carrier's mobility/density, decreasing its conductance. The improved electrical response is a consequence of the Schottky barrier height modulation as a result of the variation of the space charge density at the NF/DNP-CNT interface.[11] The proposed synergistic effect could be corroborated by electrical impedance characterization (Figure S6), which shows that, in the hybrid material, the DNP-CNT phase has a more capacitive contribution, whereas the NF phase has a major resistive character, as previously discussed.[44] It is important to emphasize that the sensor


https://doi.org/10.1021/acssensors.1c00812
ACS Sens. 2021, 6, 2457−2464

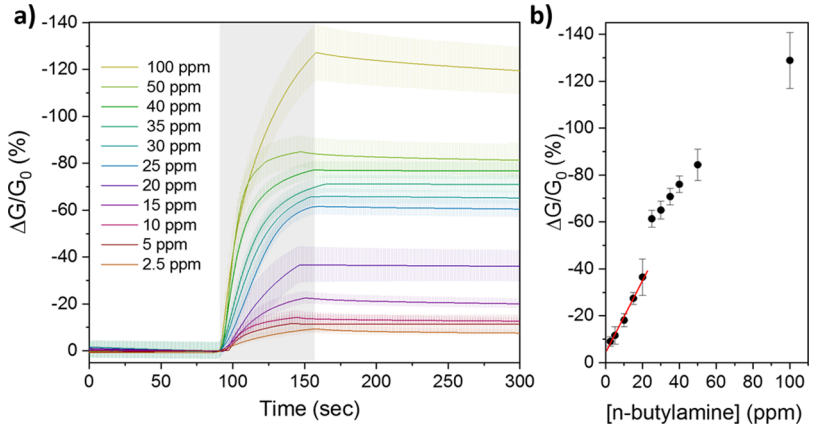


**Figure 3.** (a) Dynamic sensor response curves for NF/DNP-CNT over exposure to different concentrations of *n*-butylamine for 1 min. (b) Calibration curve of NF/DNP-CNT showing two linear response ranges.

displays an irreversible response, and this dosimetric behavior is further confirmed by three sequential exposures to 50 ppm *n*-butylamine (Figure S8a), resulting in a sensitivity decrease of ∼93%. A response time of 23 s is needed for the sensor to reach 90% of total response ($T_{90}$) to 50 ppm *n*-butylamine (Figure S8b).

A calibration curve was obtained by exposing an NF/DNP-CNT sensing unit to different concentrations (2.5−100 ppm) of *n*-butylamine (Figure 3). Dynamic curves for all concentrations confirm the irreversible response after 1 min of exposure to *n*-butylamine (Figure 3a). The calibration curve showed two linear regimes, one at lower concentrations (2.5−25 ppm) and another at higher concentrations (30−100 ppm) (Figure 3b). This response profile may be explained by the decrease in the number of active sites exposed on the outermost layer, requiring the gas to percolate into the 3D NF/DNP-CNT network to reach new active sites. The linear range at lower concentrations of *n*-butylamine can be fit to $\Delta G/G_0$ (%) = −1.223[*n*-butylamine](ppm) − 5.815 ($R^2$ = 0.9939). The limit of detection was estimated to be 20 ppb based on a signal-to-noise ratio of three (S/N = 3) following the methodology described by Fong et al.[45] The response is conserved for relative humidity (RH) values of 10 and 25%, and a decrease of ∼20% in the response to 50 ppm *n*-butylamine is observed with RH values of 45 and 65% (Figure S8c).

The NF/DNP-CNT sensitivity and selectivity were evaluated by testing with ammonia and propylamine, diethylamine, and triethylamine (Figure 4a). The sensitivity of the NF/DNP-CNT chemiresistors to organic amines is a function of the alkyl substitution. Kinetics and equilibrium constants of Meisenheimer complexes formed with different amines have been explored previously in the literature, showing such order of preference including the lower sensitivity to ammonia.[46] The selectivity toward organic volatile compounds (VOCs) was determined and is presented in Figure 4b. Our hybrid material presents an excellent selectivity to amino compounds against various VOCs. The device response is more than 40 times higher for *n*-butylamine compared, for instance, with EtOAc and THF.

After characterizing the NF/DNP-CNT chemiresistor's amine sensitivity, we integrated this material into the circuit of an RFID tag for wireless sensing studies. To ensure a monotonic variation in the RF reflection signal at the frequency of the original device, the chemiresistor (Rs) was

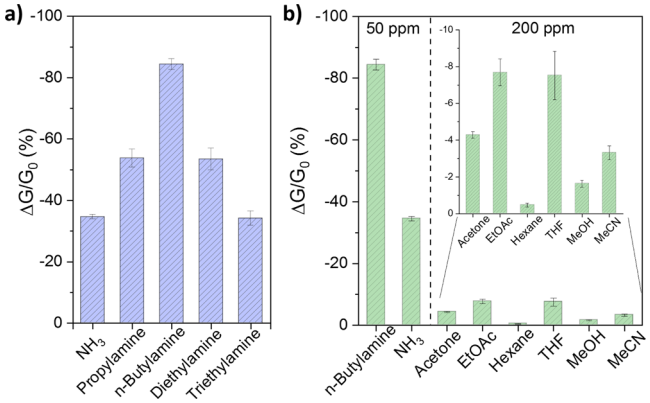


**Figure 4.** (a) Average NF/DNP-CNT device responses ($n \geq 5$) to 50 ppm amine exposures. (b) NF/DNP-CNT selectivity as revealed by the responses to 200 ppm of various VOCs in comparison with the responses to 50 ppm *n*-butylamine and ammonia. Each device was exposed to the analyte for 1 min.

added to the RFID tag using the protocol developed by Zhu et al.,[21] as described in the SI to obtain what is referred to as a *p*-CARD. The reflection signal magnitude of the wireless device is referred to as "Gain" and is determined at 13.57 MHz (S11), which is the resonant frequency minimum gain value, given in dB (numerically negative).[47] An advantage of using this protocol with RFID tags is the large gain response region wherein the resistances of the chemiresistor layer vary from 0.1 kΩ to 1 MΩ.[22] This same range was found in our NF/DNP-CNT electrical impedance measurements (Figure S6).

We employed the *p*-CARD in packages for meat to create a simulated real-world application. Gain was monitored during the room temperature storage for beef, chicken, and fish samples (Figure 5a). The gain values displayed only small changes during the first 12 h, indicating a low concentration of volatile amines. However, after 24 h of storage, the gain showed a more pronounced decrease for beef samples and became relatively constant from 36 to 80 h. Fish samples, which are known to give large amine signatures, showed changes in gain for up 72 h. For chicken samples, the gain shows a significant decrease, reaching gain values lower than −1 dB, which is the threshold levels of detection using smartphone communication (indicated by the gray area in Figure 5). These results indicate the potential of NF/DNP-CNT *p*-CARD wireless sensors for monitoring meat quality if


https://doi.org/10.1021/acssensors.1c00812
ACS Sens. 2021, 6, 2457−2464

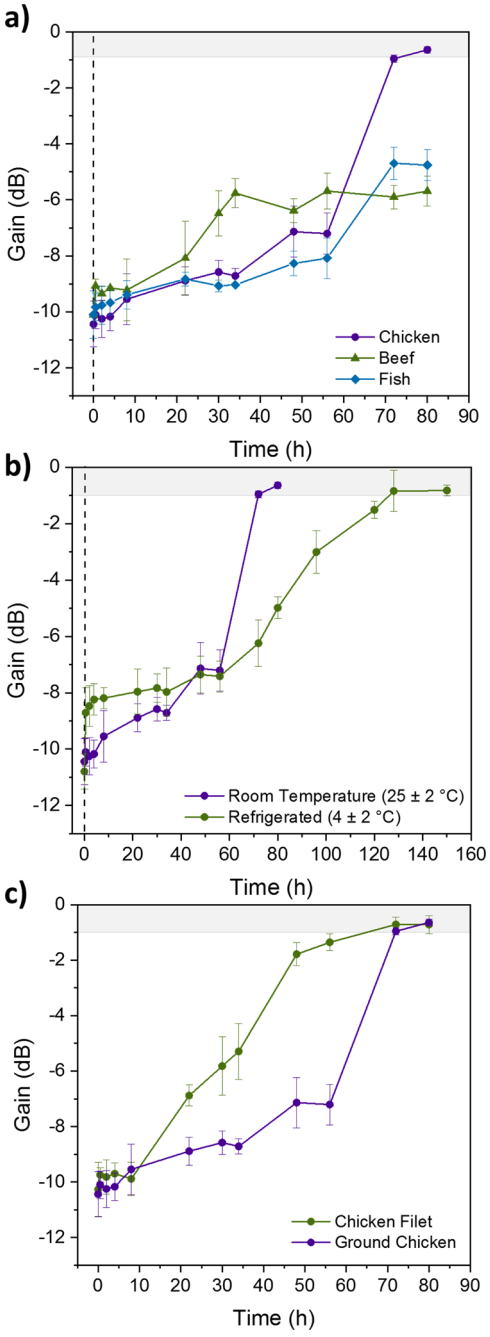


**Figure 5.** Gain plot over storage time of (a) different kinds of meats (chicken, beef, and fish), (b) chicken stored at different temperatures, and (c) different cuts of chicken meat (ground and filet cuts).

an application is developed that reveals the signal (gain) level. The more pronounced *p*-CARD attenuation for chicken (compared to fish and beef) might be explained by the difference in the degradation process. The literature has demonstrated that chicken usually emits a higher concentration of amines with higher volatility, whereas beef will present solid amines (e.g., cadaverine and tyramine) in higher concentrations.[48,49] We emphasize that the *p*-CARD was only monitoring the package atmosphere without physical contact with the meat. Quantification of total amines and volatile/solid amine ratios in meat over time of storage can be performed by gas chromatography as the work presented by Wojnowski and co-workers.[50]

It is worth recalling that both metal oxide and carbon nanotube electrical properties are susceptible to the operating temperature and, in most cases, will present better performance at higher temperatures.[51] Considering the proposed application as a sensor for raw meat quality and the material behavior susceptibility to temperature, an investigation of the storage temperature influence on chicken quality and sensor response was also conducted and is displayed in Figure 5b. Chicken stored at low temperatures (4 ± 2 °C) showed complete attenuation of *p*-CARD gain after 128 h. The gain (dB) displays a variation of ∼20% within the first hour of experiments, while at room temperature, the gain remained approximately the same (∼9.5 dB) for the initial 2 h. Such a decrease in gain observed for the low temperature test can be interpreted as an indication of temperature influence on the sensor response since negligible spoilage is expected under both conditions for such a short period of time. These initial studies were conducted with ground meat that was equally distributed in the package container (Figure S3a), and to survey other form factors, we investigated chicken filets. As presented in Figure 5c, filet cuts show a more pronounced attenuation of gain values. We were initially surprised by the faster generation of biogenic amines from filet cuts, and we rationalized that this is caused by the surfaces exposed prior to the experiment, whereas the ground chicken had the fresh inner meat being exposed to oxygen within the containers.

Although the *p*-CARD worked very well for monitoring meat spoilage over time in storage, the gain changes are not consistent with DC electric resistance measurements upon amine exposure. Motivated to better understand NF/DNP-CNT chemiresistor behavior at high frequencies, we measured the AC electric impedance of NF/DNP-CNT chemiresistors at various concentrations of ammonia. Figure 6a shows a frequency-dependent behavior and inverts the sensing response depending on the frequency range. At lower frequencies, the resistance increases with amine concentration, corroborating DC measurements performed with *n*-butylamine; however, at higher frequencies, the resistance decreases with amine concentration, corroborating with gain changes when exposed to meat. These findings indicate that for NF/DNP-CNT, it is not only the chemiresistor resistance (Rs) that governs the *p*-CARD gain, but also there is a contribution from the entire complex impedance spectrum. This behavior can also be explained by the synergistic contribution of both $SiO_2$:ZnO NF, which provides the resistive component, and the DNP-CNT, which provide the capacitive component. The $R/R_0$ ratio for the entire spectrum was determined (Figure 6b), and a linear relation is found with concentration of ammonia at 1 MHz (a frequency close to 13.57 MHz where the smartphone operates). Specifically, the ammonia concentration could be determined from the equation $R/R_0 = 0.5282 - 0.25 \log[NH_3]$, $R^2 = 0.99943$, as depicted in the inset of Figure 6b.

Considering these significant differences in response depending on the frequency, the $R/R_0$ ratio was determined at 1 MHz during chicken meat storage (Figure 7, right *Y* axis). The $R/R_0$ ratio could be related to the linear relationship between the $R/R_0$ ratio and $\log[NH_3]$, indicating a concentration of 114 ppm ammonia at 72 h of storage (the time when a smartphone signal is below the detection limits). It is worth noting that NF/DNP-CNT display lower sensitivity to ammonia than to other higher-molecular-weight amines. This indicates that the same gain change will be reached with lower concentrations of other amines.


https://doi.org/10.1021/acssensors.1c00812
ACS Sens. 2021, 6, 2457−2464

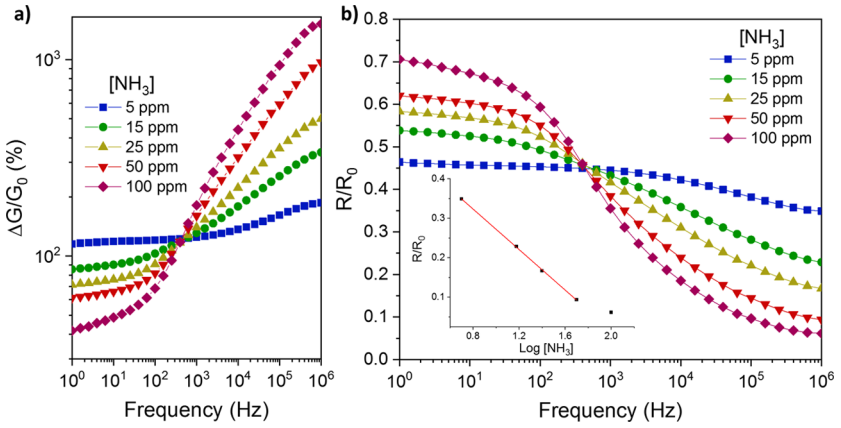


**Figure 6.** NF/DNP-CNT sensitive response to ammonia as a function of frequency as (a) conductance variation ($\Delta G/G0$ (%)) and (b) $R/R_0$ ratio. The inset in (b) presents the linear relation between $R/R_0$ and log[$NH_3$] at 1 MHz.

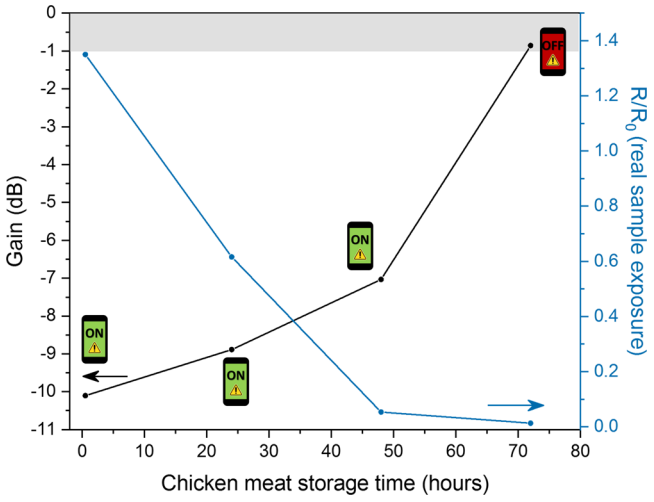


**Figure 7.** *p*-CARD gain (left *Y* axis, black curve) and $R/R_0$ ratio (right *Y* axis, blue curve) as a function of chicken meat storage. Smartphone representation of active identification of *p*-CARD (green screen) and below the detection limit (red screen).

## CONCLUSIONS

Herein, we presented a hybrid (inorganic n-type/organic p-type) chemiresistor based on $SiO_2$:ZnO nanofibers and single-walled carbon nanotubes functionalized with 3,5-dinitrophenyl functional groups for wireless sensing of biogenic amines emitted from decaying meat. The chemiresistor showed a dosimetric response for volatile amines and excellent selectivity relative to representative VOCs. The chemiresistor was incorporated into a resonant radio-frequency tag, resulting in a wireless amine sensor (NF/DNP-CNT *p*-CARD). It was shown that the reflection signal (gain) of the *p*-CARD decreased in response to chicken meat exposure with extended storage. We also showed that the complex impedance variation of the sensor response is a function of frequency and suggested that this unusual feature has its origins in the hybrid nature of the materials in the chemiresistor. Furthermore, a smartphone app was used for binary (on → off) identification of the *p*-CARD at different cumulative amine exposures, thereby indicating that this method can give rise to portable, low-cost, reliable, and easy-to-operate wireless chemical sensors for on-site food quality monitoring.

## ASSOCIATED CONTENT

### Supporting Information

The Supporting Information is available free of charge at https://pubs.acs.org/doi/10.1021/acssensors.1c00812.

Instrumentation and materials details; nanofiber fabrication; covalently functionalized SWCNT synthesis; device fabrication, optimization, and characterization; and real sample analysis description and additional photographs of meat package (PDF)

## AUTHOR INFORMATION


### Corresponding Authors

**Rafaela S. Andre** − *Department of Chemistry and Institute for Soldier Nanotechnologies, Massachusetts Institute of Technology, Cambridge, Cambridge, Massachusetts 02139, United States; Nanotechnology National Laboratory for Agriculture (LNNA), Embrapa Instrumentação, 13560-970 São Carlos, São Paulo, Brazil*; Email: rafaela.s.a@outlook.com

**Daniel S. Correa** − *Nanotechnology National Laboratory for Agriculture (LNNA), Embrapa Instrumentação, 13560-970 São Carlos, São Paulo, Brazil*; orcid.org/0000-0002-5592-0627; Email: daniel.correa@embrapa.br

**Timothy M. Swager** − *Department of Chemistry and Institute for Soldier Nanotechnologies, Massachusetts Institute of Technology, Cambridge, Cambridge, Massachusetts 02139, United States*; orcid.org/0000-0002-3577-0510; Email: tswager@mit.edu

### Authors

**Quynh P. Ngo** − *Department of Chemistry and Institute for Soldier Nanotechnologies and Department of Materials Science and Engineering, Massachusetts Institute of Technology, Cambridge, Cambridge, Massachusetts 02139, United States*

**Lucas Fugikawa-Santos** − *Institute of Geosciences and Exact Sciences, São Paulo State University (UNESP), 13506-700 Rio Claro, São Paulo, Brazil*; orcid.org/0000-0001-7376-2717

Complete contact information is available at: https://pubs.acs.org/10.1021/acssensors.1c00812


### Notes

The authors declare no competing financial interest.



https://doi.org/10.1021/acssensors.1c00812
ACS Sens. 2021, 6, 2457−2464

## ■ ACKNOWLEDGMENTS

This work was supported by the National Science Foundation DMR-1809740. The authors acknowledge Ru-Qiang Lu for the insightful discussions. D.S.C. and R.S.A. also thank FAPESP (grant numbers: 2019/04154-9, 2016/23793-4, 2017/12174-4, and 2018/22214-6), MCTI-SisNano and Rede Agronano (EMBRAPA) from Brazil.

## ■ REFERENCES

(1) Nishikawa, M.; Murata, T.; Ishihara, S.; Shiba, K.; Shrestha, L. K.; Yoshikawa, G.; Minami, K.; Ariga, K. Discrimination of Methanol from Ethanol in Gasoline Using a Membrane-Type Surface Stress Sensor Coated with Copper(I) Complex. *Bull. Chem. Soc. Jpn.* **2021**, *94*, 648−654.

(2) Kumar, V.; Kim, K.-H.; Kumar, P.; Jeon, B.-H.; Kim, J.-C. Functional Hybrid Nanostructure Materials: Advanced Strategies for Sensing Applications toward Volatile Organic Compounds. *Coord. Chem. Rev.* **2017**, *342*, 80−105.

(3) Lin, T.; Lv, X.; Hu, Z.; Xu, A.; Feng, C. Semiconductor Metal Oxides as Chemoresistive Sensors for Detecting Volatile Organic Compounds. *Sensors* **2019**, *19*, 233.

(4) Van Denburgh, K. L.; Liu, Y.; Sadhukhan, T.; Benson, C. R.; Cox, N. M.; Erbas-Cakmak, S.; Qiao, B.; Gao, X.; Pink, M.; Raghavachari, K.; Flood, A. H. Multi-State Amine Sensing by Electron Transfers in a BODIPY Probe. *Org. Biomol. Chem.* **2020**, *18*, 431−440.

(5) Feddern, V.; Mazzuco, H.; Fonseca, F. N.; de Lima, G. J. M. M. A Review on Biogenic Amines in Food and Feed: Toxicological Aspects, Impact on Health and Control Measures. *Anim. Prod. Sci.* **2019**, *59*, 608.

(6) Tseng, S. Y.; Li, S. Y.; Yi, S. Y.; Sun, A. Y.; Gao, D. Y.; Wan, D. Food Quality Monitor: Paper-Based Plasmonic Sensors Prepared Through Reversal Nanoimprinting for Rapid Detection of Biogenic Amine Odorants. *ACS Appl. Mater. Interfaces* **2017**, *9*, 17306−17316.

(7) Ruiz-Capillas, C.; Herrero, A. Impact of Biogenic Amines on Food Quality and Safety. *Foods* **2019**, *8*, 62.

(8) Biji, K. B.; Ravishankar, C. N.; Venkateswarlu, R.; Mohan, C. O.; Gopal, T. K. S. Biogenic Amines in Seafood: A Review. *J. Food Sci. Technol.* **2016**, *53*, 2210−2218.

(9) Bulushi, I. A.; Poole, S.; Deeth, H. C.; Dykes, G. A. Biogenic Amines in Fish: Roles in Intoxication, Spoilage, and Nitrosamine Formation—A Review. *Crit. Rev. Food Sci. Nutr.* **2009**, *49*, 369−377.

(10) Suzzi, G.; Torriani, S. Editorial: Biogenic Amines in Foods. *Front. Microbiol.* **2015**, *6*, 1−2.

(11) Liu, S. F.; Petty, A. R.; Sazama, G. T.; Swager, T. M. Single-Walled Carbon Nanotube/Metalloporphyrin Composites for the Chemiresistive Detection of Amines and Meat Spoilage. *Angew. Chem., Int. Ed.* **2015**, *54*, 6554−6557.

(12) Hu, Y.; Ma, X.; Zhang, Y.; Che, Y.; Zhao, J. Detection of Amines with Fluorescent Nanotubes: Applications in the Assessment of Meat Spoilage. *ACS Sensors* **2016**, *1*, 22−25.

(13) Yousefi, H.; Su, H.-M.; Imani, S. M.; Alkhaldi, K. M.; Filipe, C. D.; Didar, T. F. Intelligent Food Packaging: A Review of Smart Sensing Technologies for Monitoring Food Quality. *ACS Sensors* **2019**, *4*, 808−821.

(14) Schroeder, V.; Evans, E. D.; Wu, Y.-C. M.; Voll, C.-C. A.; McDonald, B. R.; Savagatrup, S.; Swager, T. M. Chemiresistive Sensor Array and Machine Learning Classification of Food. *ACS Sensors* **2019**, *4*, 2101−2108.

(15) Ruiz-Garcia, L.; Lunadei, L.; Barreiro, P.; Robla, I. A Review of Wireless Sensor Technologies and Applications in Agriculture and Food Industry: State of the Art and Current Trends. *Sensors* **2009**, *9*, 4728−4750.

(16) Ong, K. G.; Grimes, C. A.; Robbins, C. L.; Singh, R. S. Design and Application of a Wireless, Passive, Resonant-Circuit Environmental Monitoring Sensor. *Sensors Actuators A Phys.* **2001**, *93*, 33−43.

(17) Potyrailo, R. A.; Surman, C.; Nagraj, N.; Burns, A. Materials and Transducers Toward Selective Wireless Gas Sensing. *Chem. Rev.* **2011**, *111*, 7315−7354.

(18) Kassal, P.; Steinberg, M. D.; Steinberg, I. M. Wireless Chemical Sensors and Biosensors: A Review. *Sens. Actuators, B* **2018**, *266*, 228−245.

(19) Perret, E. *Radio Frequency Identification and Sensors*; John Wiley & Sons, Inc.: Hoboken, NJ, USA, 2014; Vol. *9781848217*, DOI: 10.1002/9781119054016.

(20) Azzarelli, J. M.; Mirica, K. A.; Ravnsbæk, J. B.; Swager, T. M. Wireless Gas Detection with a Smartphone via Rf Communication. *Proc. Natl. Acad. Sci.* **2014**, *111*, 18162−18166.

(21) Zhu, R.; Azzarelli, J. M.; Swager, T. M. Wireless Hazard Badges to Detect Nerve-Agent Simulants. *Angew. Chem., Int. Ed.* **2016**, *55*, 9662−9666.

(22) Zhu, R.; Desroches, M.; Yoon, B.; Swager, T. M. Wireless Oxygen Sensors Enabled by Fe (II)-Polymer Wrapped Carbon Nanotubes. *ACS Sensors* **2017**, *2*, 1044−1050.

(23) Mirica, K. A.; Azzarelli, J. M.; Weis, J. G.; Schnorr, J. M.; Swager, T. M. Rapid Prototyping of Carbon-Based Chemiresistive Gas Sensors on Paper. *Proc. Natl. Acad. Sci.* **2013**, *110*, E3265−E3270.

(24) Bakos, L. P.; Justh, N.; Moura da Silva Bezerra da Costa, U. C.; László, K.; Lábár, J. L.; Igricz, T.; Varga-Josepovits, K.; Pasierb, P.; Färm, E.; Ritala, M.; Leskelä, M.; Szilágyi, I. M. Photocatalytic and Gas Sensitive Multiwalled Carbon Nanotube/TiO2-ZnO and ZnO-TiO2 Composites Prepared by Atomic Layer Deposition. *Nanomaterials* **2020**, *10*, 252.

(25) Lin, D.; Dong, R.; Li, P.; Li, S.; Ge, M.; Zhang, Y.; Yang, L.; Xu, W. A Novel SERS Selective Detection Sensor for Trace Trinitrotoluene Based on Meisenheimer Complex of Monoethanolamine Molecule. *Talanta* **2020**, *218*, 121157.

(26) Alizadeh, N.; Ghoorchian, A. Hybrid Optoelectrochemical Sensor for Superselective Detection of 2, 4,6-Trinitrotoluene Based on Electrochemical Reduced Meisenheimer Complex. *Anal. Chem.* **2018**, *90*, 10360−10368.

(27) Xiong, L.; Huang, X.; Liu, Y.; Pan, L. One-Step Preparation and Characterization of Core-Shell SiO2/Ag Composite Spheres by Pulse Plating. *Sci. Eng. Compos. Mater.* **2017**, *24*, 423−427.

(28) Pang, Z.; Yu, J.; Li, D.; Nie, Q.; Zhang, J.; Wei, Q. Free-Standing TiO2−SiO2/PANI Composite Nanofibers for Ammonia Sensors. *J. Mater. Sci.: Mater. Electron.* **2018**, *29*, 3576−3583.

(29) Andre, R. S.; Pereira, J. C.; Mercante, L. A.; Locilento, D.; Mattoso, L. H. C.; Correa, D. S. ZnO-Co3O4 Heterostructure Electrospun Nanofibers Modified with Poly(Sodium 4-Styrenesulfonate): Evaluation of Humidity Sensing Properties. *J. Alloys Compd.* **2018**, *767*, 1022−1029.

(30) Ariga, K.; Minami, K.; Shrestha, L. K. Nanoarchitectonics for Carbon-Material-Based Sensors. *Analyst* **2016**, *141*, 2629−2638.

(31) Mallamace, F.; Corsaro, C.; Mallamace, D.; Vasi, S.; Vasi, C.; Dugo, G. The Role of Water in Protein's Behavior: The Two Dynamical Crossovers Studied by NMR and FTIR Techniques. *Comput. Struct. Biotechnol. J.* **2015**, *13*, 33−37.

(32) Jeon, I.; Peeks, M. D.; Savagatrup, S.; Zeininger, L.; Chang, S.; Thomas, G.; Wang, W.; Swager, T. M. Janus Graphene: Scalable Self-Assembly and Solution-Phase Orthogonal Functionalization. *Adv. Mater.* **2019**, *31*, 1900438.

(33) Sun, J.; Zhang, D.; Zhao, W.; Ji, Q.; Ariga, K. Enhanced Activity of Alcohol Dehydrogenase in Porous Silica Nanosheets with Wide Size Distributed Mesopores. *Bull. Chem. Soc. Jpn.* **2019**, *92*, 275−282.

(34) Mercante, L. A.; Andre, R. S.; Schneider, R.; Mattoso, L. H. C.; Correa, D. S. Free-Standing SiO 2 /TiO 2 −MoS 2 Composite Nanofibrous Membranes as Nanoadsorbents for Efficient Pb( Ii ) Removal. *New J. Chem.* **2020**, *44*, 13030−13035.

(35) Liu, G.; Huang, Z.-H.; Kang, F. Preparation of ZnO/SiO2 Gel Composites and Their Performance of H2S Removal at Room Temperature. *J. Hazard. Mater.* **2012**, *215-216*, 166−172.

(36) Lin, G.; Wang, H.; Li, X.; Lai, X.; Zou, Y.; Zhou, X.; Liu, D.; Wan, J.; Xin, H. Chestnut-like CoFe2O4@SiO2@In2O3 Nano-

composite Microspheres with Enhanced Acetone Sensing Property. *Sens. Actuators, B Chem.* **2018**, *255*, 3364−3373.
(37) Pinho, L.; Mosquera, M. J. Photocatalytic Activity of TiO2-SiO2 Nanocomposites Applied to Buildings: Influence of Particle Size and Loading. *Appl. Catal. B Environ.* **2013**, *134-135*, 205−221.
(38) Rao, A. M.; Eklund, P. C.; Bandow, S.; Thess, A.; Smalley, R. E. Evidence for Charge Transfer in Doped Carbon Nanotube Bundles from Raman Scattering. *Nature* **1997**, *388*, 257−259.
(39) Schroeder, V.; Savagatrup, S.; He, M.; Lin, S.; Swager, T. M. Carbon Nanotube Chemical Sensors. *Chem. Rev.* **2019**, *119*, 599−663.
(40) Dey, A. Semiconductor Metal Oxide Gas Sensors: A Review. *Mater. Sci. Eng., B* **2018**, *229*, 206−217.
(41) Hsu, C.-L.; Chen, K.-C.; Tsai, T.-Y.; Hsueh, T.-J. Fabrication of Gas Sensor Based on P-Type ZnO Nanoparticles and n-Type ZnO Nanowires. *Sens. Actuators, B* **2013**, *182*, 190−196.
(42) Moseley, P. T. Progress in the Development of Semiconducting Metal Oxide Gas Sensors: A Review. *Meas. Sci. Technol.* **2017**, *28*, No. 082001.
(43) Strauss, M. J. Anionic Sigma Complexes. *Chem. Rev.* **1970**, *70*, 667−712.
(44) Hong, H. P.; Kim, J. H.; Lee, C. J.; Min, N. K. In-Plane Impedancemetric Ammonia Sensing of Solution-Deposited, Highly Semiconductor-Enriched Single-Wall Carbon Nanotube Submonolayer Network Gas Sensors. *Sens. Actuators, B* **2015**, *220*, 27−32.
(45) Fong, D.; Luo, S.-X.; Andre, R. S.; Swager, T. M. Trace Ethylene Sensing via Wacker Oxidation. *ACS Cent. Sci.* **2020**, *6*, 507−512.
(46) Ota, N.; Nakada, T.; Shintani, T.; Kamitori, Y.; Okada, E. Computational Study for the Aromatic Nucleophilic Substitution Reaction on 1-Dimethylamino-2,4-Bis(Trifluoroacetyl)-Naphthalene with Amines. *Int. J. Org. Chem.* **2018**, *08*, 273−281.
(47) De Lima, G. R.; Gozzi, G.; Fugikawa-Santos, L. Lock-in Amplifier as Alternative Instrument for Reading RFID Tags in Sensing Application, DOI: 10.5281/zenodo.4697846.
(48) Vinci, G.; Antonelli, M. L. Biogenic Amines: Quality Index of Freshness in Red and White Meat. *Food Control* **2002**, *13*, 519−524.
(49) Zhai, H.; Yang, X.; Li, L.; Xia, G.; Cen, J.; Huang, H.; Hao, S. Biogenic Amines in Commercial Fish and Fish Products Sold in Southern China. *Food Control* **2012**, *25*, 303−308.
(50) Wojnowski, W.; Namieśnik, J.; Płotka-Wasylka, J. Dispersive Liquid-Liquid Microextraction Combined with Gas Chromatography−Mass Spectrometry for in Situ Determination of Biogenic Amines in Meat: Estimation of Meat's Freshness. *Microchem. J.* **2019**, *145*, 130−138.
(51) Kumar, V.; Majhi, S. M.; Kim, K.-H.; Kim, H. W.; Kwon, E. E. Advances in In2O3-Based Materials for the Development of Hydrogen Sulfide Sensors. *Chem. Eng. J.* **2021**, *404*, 126472.


https://doi.org/10.1021/acssensors.1c00812
*ACS Sens.* 2021, 6, 2457−2464